Quantum Dynamics from Classical Trajectories

Rafael S. Mattos, Saikat Mukherjee, Mario Barbatti

Quantum Dynamics from Classical Trajectories

Rafael S. Mattos,[1]* Saikat Mukherjee,[1,2] Mario Barbatti[1,3]*

[1] *Aix Marseille University, CNRS, ICR, 13397 Marseille, France*
[2] *Faculty of Chemistry, Nicolaus Copernicus University in Torun, 87100 Torun, Poland*
[3] *Institut Universitaire de France, 75231 Paris, France*

* *Corresponding author: mattos.rsouza@gmail.com, mario.barbatti@univ-amu.fr*

Abstract. Nonadiabatic molecular dynamics plays an essential role in exploring the time evolution of molecular systems. Various methods have been developed for this study, with varying accuracy and computational cost. One very successful among them is Trajectory Surface Hopping, which propagates nuclei as classical trajectories using forces from a quantum description of the electrons, and incorporates nonadiabatic effects through stochastic state changes during each trajectory propagation. A statistical analysis of an ensemble of the independent trajectories recovers the simulated system's behavior. This approach can give good results, but it is known to overlook nuclear quantum effects, leading to inaccurate predictions. Here, we present Quantum Dynamics from Classical Trajectories (QDCT), a new protocol to recover the quantum wavepacket from the classical trajectories generated by surface hopping. In this first QDCT implementation, we apply it to recover results at the Multiple Spawning level from post-processing surface hopping pre-computed trajectories. With a series of examples, we demonstrate QDCT's potential to improve the accuracy of the dynamics, correct decoherence effects, and diagnose problems or increase confidence in surface hopping results. All that comes at virtually no computational cost since no new electronic calculation is required.

1 Introduction

Nonadiabatic quantum dynamics has been studied for quite some time now,[1–3] and it has given birth to families of methods with different levels of approximation, computational efficiency, and confidence in the result.[4–8] Among them, the mixed quantum-classical dynamics methods[9] attempt to strike a balance between the efficiency and quality of the result, with multiple methods under this umbrella allowing us to treat larger systems without pre-computed potentials.

Among the families of nonadiabatic mixed quantum-classical (NA-MQC) approaches, surface hopping[7,10] is one of the most used methods,[11] partially due to its simplicity both conceptually and in implementation. The simplicity of the surface hopping method stems from the fact that each trajectory is propagated independently of the others, even though any discussion about the method's predictions can only happen for a swarm of trajectories. Despite its popularity, surface hopping is a strongly approximated theory with an *ad hoc* derivation and without a clear hierarchical path to improve its predictions[12], although some efforts have been made to mix it with other methods to create a more robust theory.[13] The independent-trajectories approximation, for example, requires implementing decoherence corrections. However, it is still unclear which is the proper way of doing it and even when to use it.[14]

Another successful NA-MQC method is Multiple Spawning,[4,15] which uses a basis of classical trajectories, usually referred to as Trajectory Basis Functions (TBFs), to propagate the Time-Dependent Schrödinger Equation (TDSE). The advantage is that the nuclei of the molecule are also treated at a quantum level. The quality of the result can be increased systematically by increasing the nuclear basis set, reaching exact results in the limit of an infinite basis set.[16] This comes at the complexity of an expanding number of trajectories, leading to an exponential growth in the number of electronic structure calculations required to propagate the dynamics.

In this work, we present Quantum Dynamics on Classical Trajectories (QDCT), a post-processing strategy to assess or improve the quality of a surface hopping simulation compared to a multiple spawning simulation at virtually no additional costs. QDCT leans on the strengths of each method. From surface hopping, we import the trajectories, which are expected to map the most important regions of the phase space. Since they are run independently, the computational cost is predictable. From multiple spawning, we import the heuristics to manage the trajectories, which are dressed by frozen Gaussians[17] and associated with a coefficient propagated using the TDSE that mediates the interaction between trajectories. In surface hopping, the properties are obtained as a simple average of all trajectories. With QDCT, the trajectories can be reweighted with the TDSE coefficients (Figure 1), and the properties can be computed similarly to conventional multiple spawning.

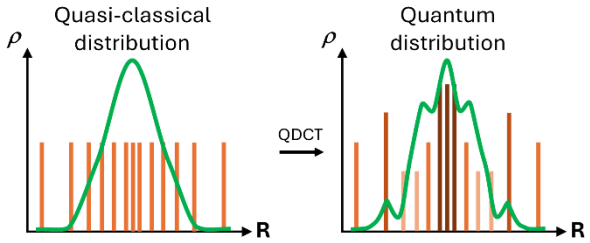

Figure 1 Conceptualization of the QDCT treatment. It can be interpreted as reweighting the pre-computed classical trajectories with the coefficients propagated using the TDSE.

Although in this first QDCT implementation, we have exclusively taken multiple spawning as the target level, this is not a restriction of the method's general idea. Any approach that uses Gaussian functions as a basis to propagate the TDSE can be replicated with QDCT. Thus, one could develop an alternative algorithm to the one presented here to propagate the widths as in Direct Dynamics variational Multi-Configurational Gaussian (DD-vMCG),[8,18] following the same principle of using pre-computed trajectories as the basis.

In this paper, we describe QDCT and its potential use cases by comparing it with multiple spawning results applied to analytical models, both unidimensional and multidimensional. In the following section (2), we explain the background theory used by the method, the equations of motion for the coefficient, and the strategies to manage the classical trajectories. Section 3 details the steps taken in implementing the method and how the theoretical concepts are put together as a complete protocol to

perform the QDCT simulation. Section 4 has the computational detail for the numerical application of the method. Section 5 presents the results of this post-process strategy applied in the unidimensional Tully models[7] and a multidimensional Spin-Boson Hamiltonian model.[19] Finally, in Section 6, we conclude and share the perspectives on the development and application of QDCT.

2 Background Theory

2.1 Fewest Switches Surface Hopping

Fewest Switches Surface Hopping (FSSH)[7] is one of the popular flavors of the surface hopping methods. In this approach, the classical particles representing the nuclei are propagated following Newton's equation of motion for each individual trajectory on a single Born-Oppenheimer electronic state. At the same time, a time-dependent electronic wave function expanded on the time-independent electronic states computed at the classical nuclear geometry is propagated with a local approximation of the TDSE. The information from the TDSE is used to determine transition probabilities between electronic states. Finally, a stochastic process chooses which state of the classical trajectory will be propagated in the next step.

At each timestep, a single-point electronic structure calculation is performed, and the generated information is used to continue the nuclear and electronic propagations, as usual in those NA-MQC methods.[9] This makes the method practical from the technical point of view since each trajectory runs individually from a set of initial conditions. The number of processors required is kept constant throughout the simulation, as stipulated by the electronic structure method. Trajectories can also be submitted at different times and on multiple computers and then copied to the same place for analysis.

Unfortunately, this advantageous and convenient independent trajectory aspect also creates limitations for the method that must be circumvented. Surface hopping considers the linear combination of the electronic states to treat the nonadiabatic effects. However, the nuclear wavepacket is represented by the swarm of independent trajectories. For each trajectory, the nuclear part is represented by a single element that does not interact with any other nuclear function. The electronic coefficients are propagated from a solution of the TDSE and determine the population in each electronic state. They are also used to estimate the hopping probability according to

$$P_{I->J} = \max\left[0, \frac{2\Delta t}{\rho_{II}}\left(\hbar^{-1}\,\mathrm{Im}(\rho_{JI}H_{JI}) - \mathrm{Re}(\rho_{JI})\mathbf{d}_{JI}\cdot\mathbf{v}\right)\right] \quad (1)$$

Within the adiabatic representation, Δt is the size of the timestep, the electronic Hamiltonian $H_{JI} = E_I\delta_{IJ}$ depends on the adiabatic potential energy E_I of state I, $\boldsymbol{v}$ is the classical velocity of the molecule, and $\mathbf{d_{IJ}} = \langle\phi_I \,|\, \nabla_{\mathbf{R}} \,|\, \phi_J\rangle_{\mathbf{r}}$ is the nonadiabatic coupling vector between state I and J, where ϕ are the electronic eigenfunctions. The index $\boldsymbol{r}$ in $\boldsymbol{d}_{IJ}$ indicates integration over the electronic coordinates. The stochastic process associated with the hopping probability is responsible for

describing the population transfer along the dynamics. The hop between surfaces is also associated with a correction in the momentum of the molecule to conserve the total energy.[20]

For a single trajectory, the reduced density matrix elements are:

$$\rho_{IJ} = c_I c_J^* \tag{2}$$

In a more general case, the off-diagonal terms of the reduced density matrix, the coherences, should also contain the overlap of the environment states,[21] which decreases with time, causing natural decoherence. In the case of an isolated molecular system, the environment is the nuclear wavepacket. This overlap will always be one for a single trajectory, which makes the surface hopping trajectories suffer from an overcoherence problem.[22] Multiple methods attempt to correct the decoherence effect lacking from FSSH while still in the context of independent trajectories.[23–25]

2.2 Multiple Spawning

Another prominent approach to simulating nonadiabatic dynamics are the multiple spawning methods: Full Multiple Spawning (FMS)[15] and *Ab Initio* Multiple Spawning (AIMS).[4,26] These methods present some significant differences compared to surface hopping, particularly in treating the nuclear degrees of freedom and the non-stochastic nature of the propagation.

FMS also uses classical trajectories to propagate the dynamics. However, they are blended into a linear combination after the propagation to approximate the nuclear wavepacket. This wavepacket is propagated quantum mechanically over this basis of classical trajectories. It is said to recover the exact nonrelativistic solution within the limit of an infinite nuclear basis.[16]

AIMS differentiates itself from FMS by employing two main approximations: the saddle-point approximation (SPA)[16] and the independent first-generation approximation (IFGA).[26,27] For the former, the matrix elements of the Hamiltonian associated with the potential energy and nonadiabatic coupling are integrals over the entire nuclear space, which is impractical for molecular applications. Instead, using the SPA, one relies on the localized nature of the Gaussian functions to compute the potential energies and couplings at the centroid position between each pair of trajectories. For the latter approximation, we expect that for systems with higher dimensionality, the trajectories rapidly move away from each other, and the overlap between them decreases quickly, making the trajectories independent. In IFGA, instead of starting the simulation from a set of initial conditions, it is a good approximation to begin a set of simulations starting from a single initial condition each.[27]

An automatic update of the number of classical trajectories that should be propagated at each timestep can control the balance between the method's accuracy and computational cost.[28,29] The population transfer between states is intermediated by a transfer between the coefficients of trajectories on different states and happens in regions with high nonadiabatic coupling. To allow for this interaction, the basis is expanded at the coupling region by spawning (adding) a new trajectory, which is at the core of the method.[15] Each trajectory being propagated is monitored, and when they enter the coupling

region, a new trajectory is created on the other electronic state with which the initial trajectory is coupled. This child trajectory is a copy of the parent when it reaches the maximum coupling value, and similar to FSSH, it has a momentum correction to keep the total energy of parent and child the same. The child is then added to the basis and is propagated on that new state.

For the propagation of the amplitudes, one uses a set of frozen Gaussians built around the classical trajectories discussed in the following section. It is possible to notice how this leads to a different treatment of the decoherence phenomena, lacking in FSSH, which is naturally accounted for by the interaction between trajectories.

One potential problem due to the automatic expansion of the nuclear basis is that the number of trajectories being propagated increases exponentially. This can be a limiting factor, especially for longer time scales. This is accompanied by the increased computational effort to perform the simulation since each classical trajectory requires electronic structure calculations at each timestep of propagation. Different methods exist to mitigate the cost, either by removing those feebly populated TBFs, having a negligible influence on the dynamics, from the entire set,[30] or by stochastically selecting a branch of trajectories to follow.[28]

2.3 Frozen Gaussians

In his seminal work on semiclassical approximation,[17] Heller proposed using a collection of frozen Gaussians to represent the nuclear wavepacket. Each Gaussian is built as a distribution centered at the position (R_i) and momenta (P_i) of a particle following a classical trajectory. The resulting wavepacket is a linear combination that can be written as

$$\Omega_J(\mathbf{R},t) = \sum_j^{N_J} C_j^J(t)\chi_j^J(\mathbf{R}),$$
$$\chi_j^J(\mathbf{R}) = \prod_{\rho=1}^{3M}\left(\frac{2\omega_\rho}{\pi}\right)^{1/4} exp[-\omega_\rho(R_\rho - \bar{R}_{j\rho}^J(t))^2 + i\bar{P}_{j\rho}^J(t)(R_\rho - \bar{R}_{j\rho}^J(t)) + i\gamma_j(t)]. \quad (3)$$

The index j counts the trajectories associated with an electronic state J. The index ρ runs over all nuclear coordinates, M is the number of atoms in the system, and N_J is the number of Gaussians associated with state J. During the propagation, the widths (ω_ρ) are specific for each atom type and are kept constant,[31] characterizing them as frozen Gaussians. The phase factor γ_j is specific for each trajectory. This combines the advantage of approximating the quantum wavepacket with the simplicity of using classical equations to propagate the trajectories.

To obtain the total wavefunction, one can use the Born-Huang expansion,[32] where for each electronic state, there is a linear combination of Gaussian functions representing the nuclear wavepacket associated with that electronic state, as in

$$\Psi(\mathbf{r},\mathbf{R},t) = \sum_J^{\infty}\Omega_J(\mathbf{R},t)\phi_J(\mathbf{r};\mathbf{R}). \quad (4)$$

The electronic functions ($\phi_J(\mathbf{r};\mathbf{R})$) are the eigenfunctions of the electronic times-independent Schrödinger equation for each electronic state J. While the trajectories are propagated using a classical equation of motion, the coefficients associated with each of them can be optimally propagated using the TDSE.

The equation of motion for the nuclear coefficients can be obtained by applying the Born-Huang wavefunction (Eq. (4)) into the TDSE. The derivation can be found in Supporting Information S1, as well as the equations for the multiple matrix elements. The resulting equation for the time derivative of the coefficients in the matrix notation is

$$\dot{\mathbf{C}} = -iS^{-1}(T-\tau+V-i\dot{S})\cdot\mathbf{C} \tag{5}$$

where

$$\begin{aligned}
S_{ij} &= \langle \chi_i^I \mid \chi_j^J \rangle_{\mathbf{R}} \delta_{IJ} \\
\dot{S}_{ij} &= \langle \chi_i^I \mid \dot{\chi}_j^J \rangle_{\mathbf{R}} \delta_{IJ} \\
T_{ij} &= \langle \chi_i^I \mid \hat{T}_n \mid \chi_j^J \rangle_{\mathbf{r},\mathbf{R}} \delta_{IJ} \\
V_{ij} &= \left\langle \chi_i^I \phi_I \middle| \hat{H}_{el} \middle| \chi_j^J \phi_J \right\rangle_{\mathbf{r},\mathbf{R}} \\
\tau_{ij} &= \frac{1}{M} \langle \chi_i^I \mid \mathbf{d}_{IJ} \cdot \nabla_{\mathbf{R}} \mid \chi_j^J \rangle_{\mathbf{R}}
\end{aligned} \tag{6}$$

The matrix S contains information on the overlap between different Gaussians, $\dot{S}$ contains the product of one Gaussian with the time derivative of another, T contains the nuclear kinetic energy, V is the potential energy and τ_{ij} has information on the nonadiabatic coupling, which connects trajectories in different electronic states using $\boldsymbol{d}_{IJ}$. The index $\boldsymbol{r}$ denotes integration over the electronic coordinates, while the index $\boldsymbol{R}$ denotes integration over the nuclear coordinates.

Other than the trajectory coefficients, the phase factors also depend on time. The phase is independent of the coordinates and is associated with each trajectory, making it redundant with the coefficient.[33,34] This grants freedom of choice for the equation of motion for the phase, which can be used to improve the stability of the coefficient integration. Here, we choose the phase propagation[35]

$$\dot{\gamma}_i = \sum_{\rho}^{3N} \frac{P_{i\rho}^2 - \omega_\rho}{2M_\rho} - E_i \tag{7}$$

so that the nuclear coefficient remains constant unless it exchanges population with any other trajectory. That is, when the overlap with all other trajectories is null or very close to zero, the real and imaginary parts of the coefficients will not exchange value. This means that the diagonal elements of the resulting matrix multiply the coefficients on the right side of Eq. (5) are zero, and the amplitude variation is only due to population transfer.

After the propagation of the swam of trajectories, one has the set of coefficients for each trajectory at each timestep. Those can be used to construct the expectation value of an arbitrary operator ($\hat{O}$) with the general form:[36]

$$\begin{aligned} O(t) &= \frac{\left\langle \Psi(t) \middle| \hat{O} \middle| \Psi(t) \right\rangle_{R,r}}{\left\langle \Psi(t) \middle| \Psi(t) \right\rangle_{R,r}} \\ &= \frac{1}{N_{ini}} \sum_{\beta}^{N_{ini}} \sum_{JI}^{N_{state}} \sum_{ji}^{N_J^\beta(t) N_I^\beta(t)} \left(c_{j\beta}^J(t)\right)^* c_{i\beta}^I(t) \left\langle \phi_J^\beta \chi_{j\beta}^J(t) \middle| \hat{O} \middle| \phi_I^\beta \chi_{i\beta}^I(t) \right\rangle_{R,r} \end{aligned} \tag{8}$$

Under the IFGA, β runs over the different initial conditions, which are assumed to be a single trajectory independent from the other initial conditions for each simulation. In particular, the electronic population can be computed as the projection into each electronic state:

$$\hat{O} = \left| \phi_I^\beta \right\rangle \left\langle \phi_I^\beta \right| \tag{9}$$

which can be used to compute the population of the electronic state *I*.

2.4 BAT approximation

Evaluating the matrix elements constituting the Hamiltonian is necessary to propagate the coefficients. In particular, we need to compute the potential energy (V_{ij}) and the nonadiabatic (τ_{ij}) terms, which can be performed using the SPA. Considering the localized nature of the Gaussian functions, the expected value of a function of $\boldsymbol{R}$ can be approximated by the product of the overlap between the two Gaussians times the function evaluated at the centroid position of the two Gaussians as

$$\langle \chi_i^I \mid f(\mathbf{R}) \mid \chi_j^J \rangle \approx \langle \chi_i^I \mid \chi_j^J \rangle f(\bar{\mathbf{R}}) \tag{10}$$

We will treat only the nuclear integrals, leaving the integration coordinate implicit.

When propagating the trajectories using SPA, it is necessary to compute the electronic properties at the positions of the trajectories for the classical propagation of the nuclei and another set of evaluations to compute the matrix elements using the SPA. An alternative is to use bra-ket averaged Taylor expansion[37] (BAT) to approximate those integrals without calculating the values at the centroid points.

For potential energy, where the energy gradients are also available, the first-order Taylor expansion is expressed as

$$V_{ij} \approx \frac{V_I(\bar{\mathbf{R}}_i) + V_I(\bar{\mathbf{R}}_j)}{2} S_{ij} + \frac{\langle \chi_i \mid \mathbf{R} - \bar{\mathbf{R}}_j \mid \chi_j \rangle \nabla_R V_I(\bar{\mathbf{R}}_j) + \langle \chi_i \mid \mathbf{R} - \bar{\mathbf{R}}_i \mid \chi_j \rangle \nabla_{\mathbf{R}} V_I(\bar{\mathbf{R}}_i)}{2} \tag{11}$$

can be used, which already considers that the potential energy term is only nonzero when both trajectories evaluated are in the same electronic state.

Similarly, we can use the zeroth-order Taylor expansion to approximate the nonadiabatic coupling matrix element

$$\tau_{ij} \approx \frac{d_{IJ}(\overline{\mathbf{R}}_i) + d_{IJ}(\overline{\mathbf{R}}_j)}{2M} \langle \chi_i^J \mid \frac{\partial}{\partial R} \mid \chi_j^J \rangle. \tag{12}$$

The BAT approximation has shown good results[37] while significantly reducing the amount of electronic structure computations. In the context of QDCT, this approximation allows us to propagate the nuclear coefficients using only the information generated by regular surface hopping dynamics without requiring extra electronic structure calculations at the centroid points.

3 Quantum Dynamics on Classical Trajectories

Looking at the equations of motion of the trajectories in multiple spawning, it can be realized that each trajectory is not dependent on the rest of the nuclear basis. This implies that they do not need to be propagated simultaneously. Other than the fact that the spawned trajectories will only appear when the parents reach a specific point in time, each trajectory can be propagated independently. After that, the coefficients can be propagated. This opens the way for new approaches, like using pre-computed trajectories from surface hopping and only propagating the coefficients.

The trajectories generated by surface hopping have some distinctions compared to those generated by conventional multiple spawning. The most obvious one is that the AIMS trajectories remain in the same state throughout their existence. In contrast, the FSSH trajectories will eventually change state due to the hoppings, occasionally multiple times in a single trajectory. This distinction creates a problem of discontinuities of trajectories that must be addressed if one intends to use them for coefficient propagation. The other and more subtle distinction is that the spawned trajectories are created at the ideal point in space and time to maximize the overlap between trajectories, favoring their communication and allowing the TDSE to control the population transition. The FSSH trajectories are not subjected to this constraint, creating an increasingly impeditive problem for computing the overlap as the dimension of the system increases.

On the other hand, using pre-computed trajectories means that the electronic structure calculations do not need to be repeated, so one obtains an approximation of a multiple spawning calculation at the cost of computing an analytical model. It is also easier to control the computational cost of running multiple independent trajectories since the cost of each trajectory is easy to predict. The proposition is not a method to replace AIMS calculations but a correction to existing surface hopping dynamics that can work as a guide to assess the quality of the original calculation. Other methods employ the exploration of classical trajectories.[38] However, in those cases, the trajectories exist in the function of the coefficient propagation. In QDCT, the pre-computed trajectories are a valid dynamic by themselves. The difference between the results before and after QDCT can point to potential shortcomings of surface hopping, while the similarity between them can increase confidence in the result at almost no extra cost.

The classical trajectories are used similarly to a conventional AIMS simulation. They are dressed with frozen Gaussians to create the nuclear wavepacket, and the equations of motion for the coefficients are

presented in Section 2.3. The condition for the increase in the number of trajectories being considered is also the same spawning condition mentioned previously. A threshold for the nonadiabatic coupling is established to define the coupling region. At the maximum point for this coupling value, a new trajectory is added to the nuclear basis, forming this relation between parent and child trajectories.

In our case, instead of creating a new trajectory during spawning, one of the available surface hopping trajectories is selected and added to the active nuclear basis (Section 3.2). This addition may be assisted by interpolated trajectories (Section 3.3), which use data from the pre-computed trajectories to approximate the ideal child trajectory (Figure 2).

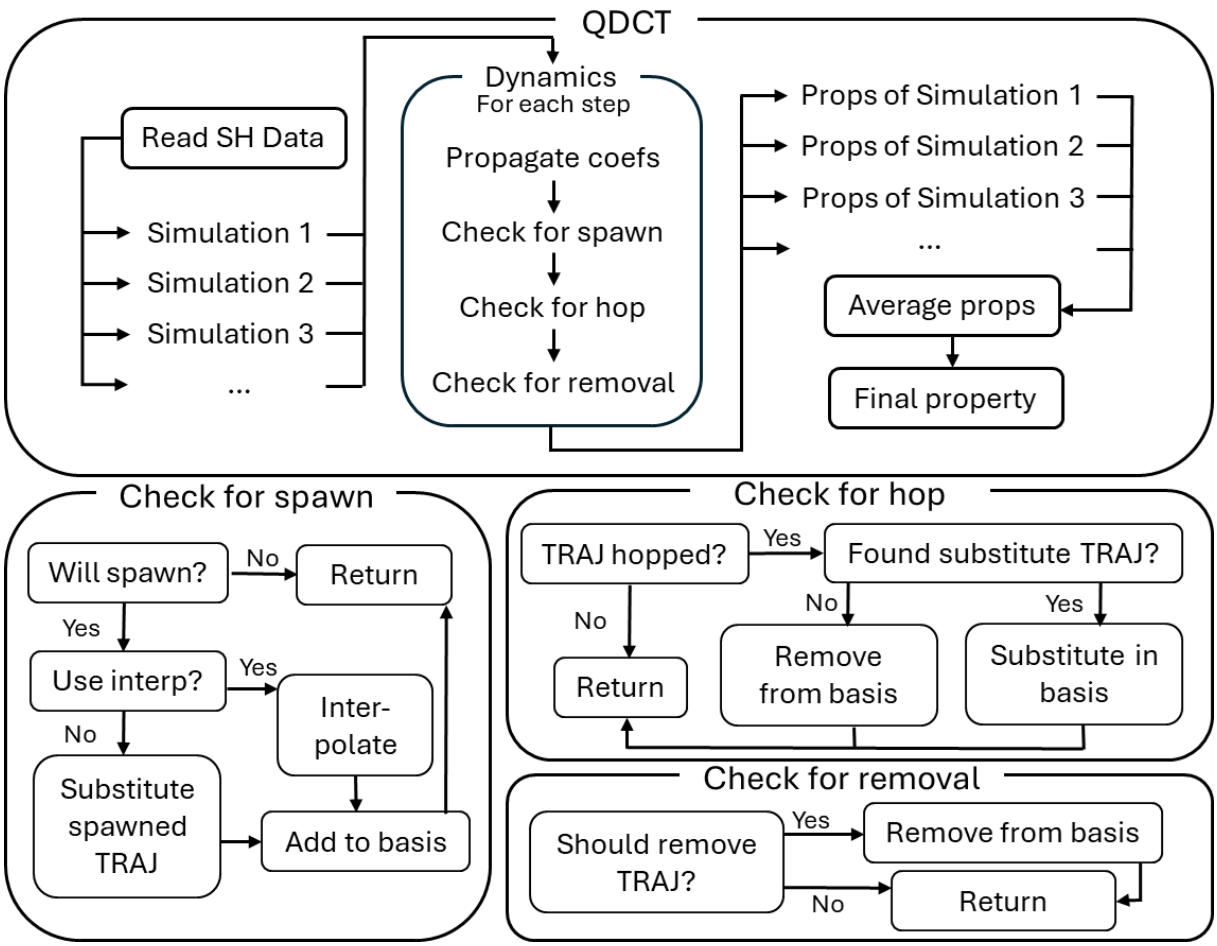

Figure 2 Flowchart of the most critical steps in QDCT. It reads the pre-computed trajectories and starts a new simulation for each trajectory. The available pre-computed trajectories can be added or removed from the active nuclear basis during the simulation.

Next, we discuss the strategies to circumvent the problems that arise when using surface hopping trajectories to propagate AIMS equations. To deal with the discontinuities caused by hoppings, we perform trajectory substitutions. When computing the overlap between parent and child trajectories, we create a pair of interpolated trajectories that approximate the spawning and lead to a smooth population transfer. We detail how the spawnings and trajectory elimination are treated and summarize

how those ideas can be combined into a single workflow that allows QDCT to correct surface-hopping results.

3.1 Trajectory Basis Functions control

The control of the number of trajectories in the nuclear basis balances the addition of trajectories by spawning and removing them. The norm of the nonadiabatic coupling vector or its product with the velocity can be monitored for each trajectory until it reaches a predefined threshold. At this point, the rest of the simulation is put on hold, and the trajectory that reaches the threshold is propagated alone until the maximum coupling value. At this time, a child trajectory is created, keeping the same geometry of the system and, consequently, the same gradients, energies, and nonadiabatic coupling. The nuclear momentum, however, is modified so that the total energy of the child and parent trajectories remains the same. This correction can be a rescale in the direction of momentum or can be performed in the direction of the nonadiabatic coupling, similar to the correction applied in FSSH,[39] following the relation

$$v_\alpha^{(J)} = v_\alpha^{(L)} + \gamma_{LJ} \frac{u_\alpha}{M_\alpha}. \tag{13}$$

In this equation, α runs over the nuclear coordinates, and $\boldsymbol{v}$ is the velocity vector in the state before the hop/parent (L) and after the hop/child (J). $\boldsymbol{u}$ is the unit vector that informs the correction direction, M_α is the mass of the coordinate α, and γ is chosen so that the total energy is conserved.

In conventional AIMS, one would backpropagate the child trajectory to the current simulation time and return the rest of the simulation to its regular run. Here, we are not propagating the classical trajectories, so instead of this backpropagation, we perform a trajectory substitution to increase the number of trajectories in the basis. The details of how this substitution happens will be discussed in Section 3.2. Still, the idea is to find the one most similar to the trajectory being substituted in the list of surface hopping trajectories. In this case, the new trajectory would fill in the role of the child being added to the nuclear basis, already considering the corrected momenta when performing the substitution. Instead of backpropagating, we add the new trajectory to the nuclear basis at the beginning of the coupling region. The surface hopping trajectory may change state between the beginning of the coupling region and the maximum coupling time. This is considered when choosing a trajectory to perform the substitution. In this case, the trajectory will be added to the nuclear basis as soon as it enters the correct state. When the trajectory is added to the simulation, its phase and coefficients are zero.

Trajectory elimination can occur for a couple of reasons, including intentionally reducing the basis size. The usual elimination performed in AIMS can remove trajectories that are not coupled with the rest of the TBFs and do not contribute to the population. In QDCT, this elimination can also happen in case of a failed substitution, when the TBF being followed needs to be replaced, but no other is found suitable to fill its role.

In the first case, when the removal is performed on purpose, there are three criteria to be observed when deciding whether the trajectory should be removed. First, one checks whether the trajectories are coupled through the Hamiltonian in the same sense as in Energy Stochastic Selection AIMS (ESSAIMS).[28] This observes both direct and indirect coupling, and one trajectory can only be considered for elimination if it is entirely uncoupled from all others. The second criterion checks whether the trajectories significantly overlap with any other TBF. If the absolute value of the overlap of the trajectory being checked with all others is smaller than a given threshold, then it can be considered for elimination. Lastly, the nuclear population of that trajectory can be computed as

$$p_i = c_i^* \sum_j^{Ntraj} \langle \chi_i^I \mid \chi_j^J \rangle c_j \tag{14}$$

If the nuclear population is below a given threshold, then it is another approval for elimination. If the trajectory has been marked for elimination at the end of all checks, it is put in observation. The dynamics continue to run normally for a given number of timesteps. At each step, the trajectory passes through the same set of checks. If it was continuously marked for elimination during the monitoring time, it is removed from the nuclear basis. Otherwise, if, at some point, any of the checks did not mark the trajectory for elimination, then it is removed from observation and continues to be treated as any other. It would have to go through the process again to be eliminated.

On the other hand, if the elimination is caused by a failed substitution, one can decide at the beginning of the script whether to attempt to continue the simulation and perform the removal or whether the run should be stopped altogether. A compromise between the two alternatives could be to evaluate the population of the trajectory being removed and how this removal would affect the norm of the wavefunction to decide on performing the elimination or stopping the simulation.

When the trajectory is removed from the nuclear basis, the nuclear wavepacket is projected into the new reduced basis to adjust the coefficients by

$$\sum_i^{Ntraj} \langle \chi_j^{(n)} \mid \chi_i^{(n)} \rangle c_i^{(n)} = \sum_k^{Ntraj} \langle \chi_j^{(n)} \mid \chi_k^{(o)} \rangle c_k^{(o)}. \tag{15}$$

The new coefficients $c_i^{(n)}$ are obtained by solving this system of equations that equates the projection of the nuclear wavepacket with the new and old TBF into the basis $\chi_j^{(n)}$. After this, there is another normalization step to ensure that each electronic state conserves the population through the elimination process and a second normalization to ensure that the total norm before and after the elimination is the same. The norm after this step is not set to unity but is conserved from whatever the value it was before the trajectory removal. If the trajectory is being removed on purpose, this renormalization step is redundant, but when the removal is imposed due to failed substitution, the projection in Eq. (15) may not go so well. In this case, the difference between the wavefunction norm before and after the removal can also be used as a criterion to decide whether to continue the simulation.

3.2 Trajectory substitution

As mentioned in Section 3.1, trajectory substitution can be applied at spawning to add the child trajectory to the simulation. Given the nature of the surface hopping trajectories, this procedure can also be necessary after the original trajectory has hopped and changed state. In the ideal case, we expect the trajectory to follow a specific state; when there is a hop, this is not the case, and it is necessary to replace this TBF with another one in the correct electronic state.

Once the trajectory that needs to be substituted has been identified, one needs only their position and momentum. One can then go through all other surface hopping trajectories in the correct state and compare the overlap between them and the one being replaced. Initially, one can attempt to compare trajectories at the same simulation time, considering that the swarm of trajectories is expected to move with the nuclear wave packet. However, this can also be extended by looking at extra steps around the current time. This can be seen as inexpensively increasing the number of TBFs, in a slightly similar philosophy as in the "trains" of trajectories.[35,40] Then, one finds the highest overlap among all trajectories within the time window chosen (Figure 3). When comparing the overlaps, one can define a minimum value worth considering and ignore trajectories that overlap below this threshold.

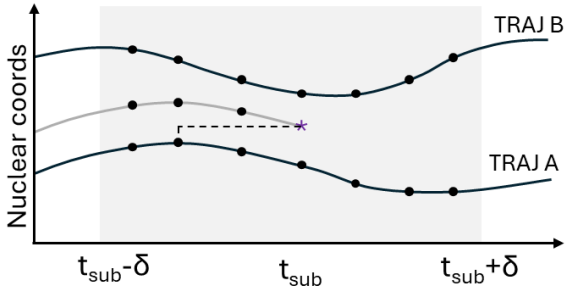

Figure 3 Schematic representation of the substitute search. The greyed-out trajectory has to be replaced. Within the same timestep, TRAJ B is the closest trajectory and will be used as a replacement; within a time window (grey region), TRAJ A is the closest, and the point at 2 steps back will be used as a replacement.

With the increase in the system's dimensionality, the chance to find a pair of trajectories with a high nuclear overlap falls dramatically. In this case, the simple overlap between pairs of trajectories will always fall below the threshold, and no substitution can be performed. In this scenario, the root mean square displacement (RMSD) can be optionally used to select trajectories. It will also use the same time window to find the best match. This alternative will always find the substitute with the highest similarity, even if it is low. Suppose this is used when replacing the spawned trajectory. In that case, this will lead to a deficit in population transfer since a trajectory that does not overlap with the child will also not overlap with the parent. On the other hand, when used after a hop to replace a trajectory

completely decoupled from the other TBFs, it does not extensively affect the final result of the simulation.

Once the trajectory has been found, be it from the overlap of the RMSD, the substitution is performed, and the new coefficients are obtained from the same type of projection mentioned for trajectory elimination (Eq. (15)).

The differences are that, in this case, the projection is a square matrix, and the diagonal element of the overlap between the trajectory being substituted and the new one is artificially set to one to ensure proper inheritance of the original population. After the projection, the same normalization procedures ensure that the electronic populations and the norm are the same as before the substitution.

In the case of a failed substitution of a child trajectory, the spawn is denied, and the simulation can be concluded as failed or continued based on the input. If it fails at a hopping, the simulation can also be finished as failed, or the trajectory being removed will be eliminated normally, with projection and normalization.

3.3 Interpolated trajectories

The increase in dimensionality of the system can usually lead to difficulties. In this case, the problem is the lack of overlap between any pair of trajectories, which depends on their positions and momenta. In traditional AIMS, this is circumvented by the spawns happening at specific points in the phase space to maximize the similarity between parent and child. This is never a criterion for a trajectory generated by usual surface hopping; consequently, the trajectories of a high-dimensional system never meet. As the interaction between coefficients depends on this overlap, either one would need an infinite number of trajectories so they can meet by chance, or the overlaps will be negligible in all cases, and the trajectories will never interact. This prohibitive condition invites the use of another approximation to make it feasible to treat large systems.

Virtual trajectories can artificially increase the number of TBFs and allow them to be added in the most critical regions of the phase space. Multiple ways to create those virtual trajectories can be imagined: the new points can be interpolated from a single trajectory, or they could be interpolated from the closest trajectories in the phase space. Alternatively, instead of simply interpolating the points of the trajectories, the actual energy surface around the spawning region could be fitted from the geometries pre-computed around it,[41] and the virtual trajectory could be propagated over this fitted potential surface. With the development of machine learning potentials,[42] we could reach a point where they are automated enough that a simple model, valid only for a short region of the phase space where the virtual trajectories are required, could be trained from the other pre-computed trajectories. Both the fitting or training of machine learning potential would be restricted to a small part of the phase space, which could potentially make those approaches computationally viable. Alternatively, one could only compute new electronic structure calculations for a reduced number of points within the coupling region. However, in this work, we want to test the method without requiring new single-point

calculations. Also, while machine learning potentials have been gaining traction, they are still not straightforward enough to be used as a black box method. We will then focus only on the most straightforward and inexpensive interpolation to show the potential of the idea. There will always be a pair of trajectories: the parent, the trajectory pre-computed by surface hopping, and the spawned/child trajectory, which in QDCT is the virtual trajectory. Here, we choose to obtain the data of those virtual trajectories (gradients, energies, and couplings) by interpolating the data already available in the parent.

Those interpolated trajectories are the most important within the coupling region, where the interaction between parent and child trajectories controls the electronic population transfer. Starting at the maximum of the coupling region, the child trajectory (interpolated) has the same information as the parent, except for the current state of the trajectory and the momentum correction (Eq. (13)) to preserve total energy. At this point, both trajectories have their forces and momenta available, and one can then compute the distance of each atom in each coordinate as

$$\Delta r_\alpha^{(k)} = p_\alpha^{(k)} dt_{(k)} + \frac{f_\alpha^{(k)} dt_{(k)}^2}{2}, \tag{16}$$

where k represents either interpolated (i) or original (o) trajectories, and α stands for each nuclear coordinate. Since both trajectories move with different momentum (p) and force (f), they will run different distances. It is possible to determine at which time the original trajectory will match in position with the interpolated one by equating the distances traveled, as in

$$p_\alpha^{(i)} dt_{(i)} + \frac{f_\alpha^{(i)} dt_{(i)}^2}{2} = p_\alpha^{(o)} dt_{(o)} + \frac{f_\alpha^{(o)} dt_{(o)}^2}{2}. \tag{17}$$

In Eq. (17), all values are fixed except by the timestep size of the original trajectory (dt_o). This quadratic equation can be solved for the smallest positive result to obtain the time at which the values of the parent should be interpolated to get the values of the interpolated trajectory, as exemplified in Figure 4. Let us clearly state that this does not mean that the interpolated and original trajectories are moving with different timesteps. All trajectories in the simulation run with the same step size. What we are doing is, by knowing the velocity of the original trajectory, we can determine what timestep would be required for it to be in the same coordinates as the interpolated.

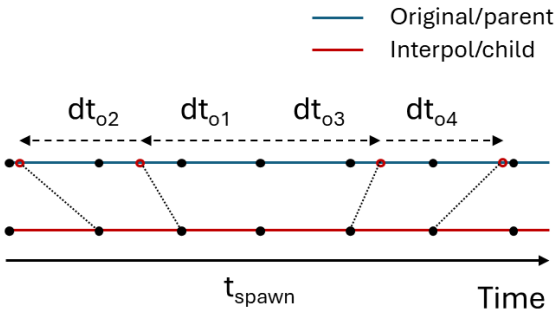

Figure 4 Scheme of creation of the interpolated trajectory using the original trajectory. In this case, the child is created in a lower state and moves faster due to momentum rescaling. The original timestep size (dt_o) is used to compute the time at which the parent and child are in the same position, and the information of the original trajectory is used to interpolate the data of the child.

With this theoretical coordinate, we can use the data around already computed to interpolate the data of the interpolated trajectory using cubic Hermite spline interpolation. For the vectorial quantities (positions, gradients), each coordinate will have an interpolation time *t*, and the interpolated value can be computed coordinate-wise, as in

$$y(t) = (2t^3 - 3t^2 + 1)y_0 + (t^3 - 2t^2 + t)\left(\frac{dy}{dt}\right)_0 + (-2t^3 + 3t^2)y_1 + (t^3 - t^2)\left(\frac{dy}{dt}\right)_1 \quad (18)$$

y(t) is the value to be interpolated, y_0 is the value on the original trajectory at the beginning of the timestep, and y_1 is the value at the end of the step. *dy/dt* are their derivatives at those same beginning and end of the timestep. The free variable *t* is normalized so that $y_0 = y(0)$ and $y_1 = y(1)$. In some coordinates, Eq. (17) might not have a solution. In this case, we can use the average timesteps of the other coordinates and perform the interpolation normally.

Eq. (17) usually returns slightly different timestep sizes for each coordinate. This can be explained by gradients in different states giving more energy to different coordinates. Using a time for each coordinate can be justified because cartesian coordinates are orthogonal, so the force applied in one coordinate will not affect the position in another. This is why the coordinate-wise interpolation was used only for positions and gradients, while momentum is computed from the gradients. At first, we experimented with an average time for all coordinates, but we noticed that the current scheme could better approximate the interpolated trajectory from the trajectory created by conventional spawning.

Not all data will have a derivative available, so we opted to use numerical derivatives in all cases:

$$\left(\frac{dy}{dt}\right)_i = \frac{y_{i+1} - y_{i-1}}{2}. \quad (19)$$

Suppose that there is a simulation with a timestep of 0.5 a.u. and the interpolation time is at 10.2 a.u. In this case, the interpolation would use:

$$
\begin{aligned}
t &= \frac{(10.2-10.0)}{0.5} = 0.4 \\
y_{-1} &= y(9.5) \\
y_0 &= y(10.0) \\
y_1 &= y(10.5) \\
y_2 &= y(11.0)
\end{aligned}
\tag{20}
$$

For the interpolation of the energies and coupling vectors, the time used is an average between all nuclear coordinates. Despite the coupling vector also being a vectorial quantity, we chose to interpolate it for a single time, where the molecule has a defined geometry instead of coordinate-wise. Once the interpolated gradients are computed in the new time, the momentum is also updated by using the usual Verlet algorithm:

$$
p_1^{(i)} = p_0^{(i)} + \frac{f_0^{(i)} + f_1^{(i)}}{2} dt \,. \tag{21}
$$

It can be noticed by looking at the Verlet algorithm and equation to propagate the coefficients in the Supporting Information S1 that for the interpolated trajectory to be possible, the parent trajectory must have the gradient in the state of the child trajectory. At this point, both the original and interpolated trajectories have all their information computed and ready to be used, the original since it was pre-computed and the new trajectory due to the interpolation. The following timesteps can be computed following the same procedure until the interpolated trajectory is no longer required.

To a reasonable degree, around the maximum coupling point, the path they are following is still similar. By the time the trajectories have drifted apart enough to decrease the quality of the interpolation, the overlap between them will have reduced and uncoupled them. All population transfer should have happened by that point, and the trajectories can be considered independent. The larger the system's dimensionality, the faster the overlap should fall and the safer the interpolated trajectory should be.

We are not interested in the interpolation for the whole trajectory, so we need some criteria to stop interpolating. First, we check if the norm of the nonadiabatic coupling of the interpolated trajectory is decreasing. The interpolation starts at the maximum coupling, so when we are propagating forward and backward in time, away from this point, the norm of the nonadiabatic coupling vector should decrease. If it reaches an inflection point and starts to rise, it will enter a new coupling region. A new interpolated trajectory should be created to describe this new region better so the current interpolated trajectory will not be propagated further in that direction. Second, it checks the overlap between the child and parent trajectories. While the overlap is high, the trajectories still interact, and the interpolation should continue. After the overlap falls below a given threshold, the norm of the nonadiabatic coupling is also checked, and the interpolation stops when this norm is smaller than the threshold that defines the beginning of the coupling region.

The interpolated trajectories are necessary only to replace the child trajectories, but in the context of surface hopping, there is a chance of hops in the coupling region. The parent is also created as an

interpolated trajectory to avoid dealing with trajectory correction and substitution within the coupling region. In the case of a hop, the parent trajectory returned will behave as if the trajectory remained in the same state for the whole coupling region.

After the interpolated trajectories are created, they are added to the nuclear basis, and the coefficient propagation continues. The child is added as a new trajectory, and the parent is added as a replacement. After the coefficient propagation passes through the coupling region, the overlap between the interpolated trajectories and all other TBFs is evaluated until they are entirely independent of the others and can be replaced again by another trajectory generated by FSSH. At this point, the substitution will not significantly overlap in higher dimensions. However, since the trajectory is independent of the other TBFs, this can still recover a good population description.

3.4 Method's workflow

We chose to start the coefficient propagation from a single trajectory. Then, multiple propagations can be performed starting from different initial conditions, similar to the IFGA. It is possible to attempt to start from various trajectories, create a reference initial wave packet to determine the initial coefficients, and perform the propagation. However, this tends to give good agreement with IFGA in higher dimensions,[27] especially considering we are working with many, primarily independent, trajectories.

Initially, we follow a single trajectory, but along the propagation, new trajectories will be added to the nuclear basis, reproducing a spawn. At each timestep, checks are performed to evaluate the need for spawning or substitution. This can be described by the following steps, which lead to the overall scheme represented in Figure 5:

1. **Coefficient propagation:** the data of the current and previous timesteps are used to propagate the coefficients (Eq. (5)) and the phase (Eq. (7)) to the current step;
2. **Trajectory substitution:** each trajectory is checked for a hop in the following step. In the case it hops, it would create a problem for the coefficient propagation, so the trajectory is substituted as described in Section 3.2, and the new coefficients are computed by Eq. (15). This is exemplified in time t_{H1} in Figure 5.
3. **Trajectory spawning:** the nonadiabatic couplings are compared with the given threshold to determine whether the trajectory (T_A) entered the spawning region. If so, it is followed until the maximum coupling point, independent from the rest of the simulation, and the pair of interpolated trajectories is created in the parent and child states(i-T_AS_0 and i-T_AS_1), as explained in Section 3.3. The values of the interpolated trajectories are interpolated from the parent trajectory (T_A) as per Eq. (18). They are added to the nuclear basis at times t_{C1} (in Figure 5) and used normally for the coefficient propagation, as any other trajectory originated from surface hopping. The interpolated trajectories are not evaluated for new spawns;

4. **Interpolated substitution:** the interpolated trajectories are interpolated only within the coupling region, so they must be replaced after this interval. The same check as in step 2 is used to replace the interpolated trajectory with another pre-computed from surface hopping at the end of the interpolation region, marked with times t_{S1} in Figure 5. Notice that in t_{S1} and t_{S4}, the interpolated is replaced by the same trajectory that originated it, so they should be a good match, while in t_{S2} and t_{S3} a new trajectory is replacing the interpolated, and there will be a difference in positions and other values between trajectories. The original trajectory might remain in the same state during the coupling region, as in t_{S1}, or might have hopped and will be replaced accordingly, as in t_{S4};

5. **Trajectory elimination:** in case of a failed substitution in step 2 or following the criteria of low population and coupling with the TBFs mentioned in Section 3.1, a trajectory can be removed, as in t_{E1} in Figure 5. At this point, the wavepacket before the removal is projected into the remaining trajectories to obtain the optimal coefficients (Eq. (15));

6. **Closing the step:** update the timestep of the classical trajectories and return to step 1 to continue the propagation.

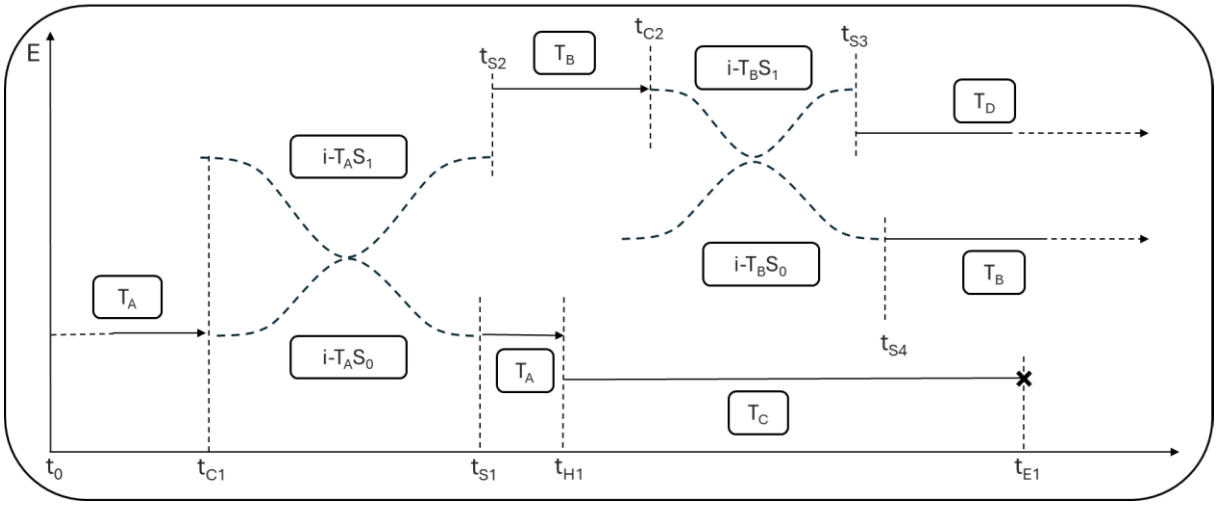

Figure 5 Schematic representation of the management of classical trajectories computed with surface hopping (T_A, T_B, T_C, and T_D) or interpolated trajectories (i-T_AS_0, i-T_AS_1, i-T_BS_0, and i-T_BS_1) during a QDCT propagation and the critical events that can happen: t_C spawning with the creation of interpolated trajectories; t_S end of coupling region with the substitution of interpolated trajectories by an original one; t_H hop of the surface hopping trajectory, triggering a substitution; t_E trajectory elimination due to low population.

This process can be started independently for all or part of the trajectories available from surface hopping. As is the case for AIMS simulations,[43] QDCT needs fewer initial conditions to converge, so starting from all the trajectories may not be necessary. After propagation, the properties of interest, such as the population, can be computed using Eq. (8), as one would do for conventional multiple

spawning. The expectation value can be computed for each simulation starting from independent initial conditions (IFGA). The final value is the simple average between multiple simulations.

4 Computational details

The FSSH calculations were performed in NewtonX v3.5.1[44] using the decoherence correction from Granucci and Persico.[45] The multiple spawning references were computed using in-house software that will soon be made available. The QDCT post-processing was performed with a code developed for this project, available at https://gitlab.com/rafaelcpii93/qdct.

For the unidimensional testing, the Tully models[7] were used (Figure 6). The trajectories are sampled from a Wigner distribution of a Gaussian wavepacket[44,46] around the position -8 a_0 for models A and B in Figure 6 and position -15 a_0 for model C. In all cases, different initial momenta were used. During the initial sampling, the width for the Gaussian followed Tully's original recommendation of $\Delta_p = 20 / p_0$. The mass was set as 2000 m_e, and the Gaussian width for both multiple spawning propagation and QDCT was chosen to be 4.7 a_0^{-2}. The trajectories start on the ground state and are propagated with a timestep of 0.1 fs. The common parameters between the multiple spawning and QDCT simulations shared the same values. The coupling threshold is achieved when the norm of the NAC vector passes the value 0.08 a.u., and the absolute value of the overlap between child and parent is 0.7 to accept a spawn. The BAT approximation was also used in the multiple spawning calculations to enable a clearer comparison with QDCT. The comparison between the BAT and SPA results can be found in Supporting Information S2. In QDCT, a time window of 60 timesteps around the simulation time was used when looking at trajectories for substitution, and the threshold of the absolute value of the overlap to accept a substitution is 0.9.

A total of 500 initial conditions were used for all calculations, starting at the lower electronic state. The same initial conditions were used for the surface hopping, multiple spawning, and, consequently, the QDCT simulations. This number of initial conditions is low for treating analytical models, which usually is in the thousands for surface hopping.[7,47,48] Nevertheless, we chose to use fewer trajectories to show the potential of the method, considering that a routine ab initio simulation tends to have between 100 and 200 trajectories.[49–51]

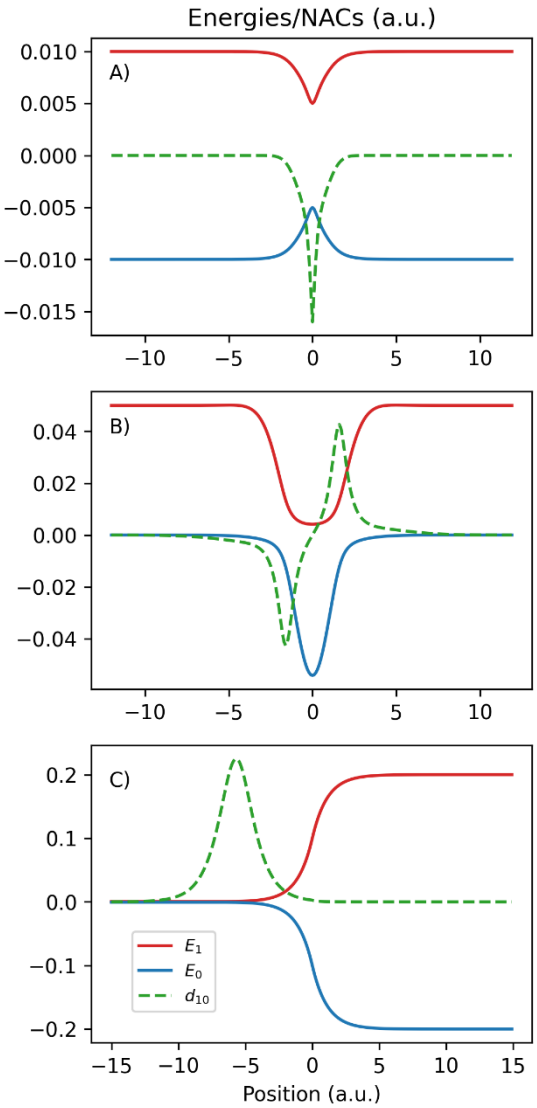

Figure 6 Tully model potentials in adiabatic representation. Energies and nonadiabatic couplings from E_1 to E_0 in a.u. The presented d_{10} values are rescaled to fit with the energies: A) Simple avoided crossing $d_{10}/100$, B) Dual avoided crossing $d_{10}/20$, and C) Extended coupling with reflection d_{10} without rescaling.

For the multidimensional test, we used the spin-boson Hamiltonian[19,52–54] model with 12 dimensions. The functional form, parameters for this system (and also the Tully models), and adiabatic transformation are found in the Supporting Information S3. In Figure 7, we present cuts of the potential energies and the norm of the nonadiabatic coupling over three coordinates: A) the coordinate associated with the lowest vibrational frequency; B) a coordinate associated with a medium-valued frequency; C) the coordinate associated with the highest frequency in the model. Other than testing QDCT in a multidimensional case, the model was parametrized such that the nonadiabatic transitions occur in 0.5 ps simulation time (a typical timescale for ultrafast photodynamics) to test the data management capability of the software.

Most parameters used in the 1D case are kept the same in the multidimensional tests. In this case, the population threshold to remove a trajectory is 0.01 in multiple spawning and QDCT. The same initial conditions were used for the multiple spawning and surface hopping dynamics for the sets with 100 and 500 trajectories. The particles used were hydrogen atoms with a mass of 1822 m_e. They were sampled from a Wigner distribution around the minimum position of the ground state with zero average initial momentum and then vertically lifted to the first excited state.

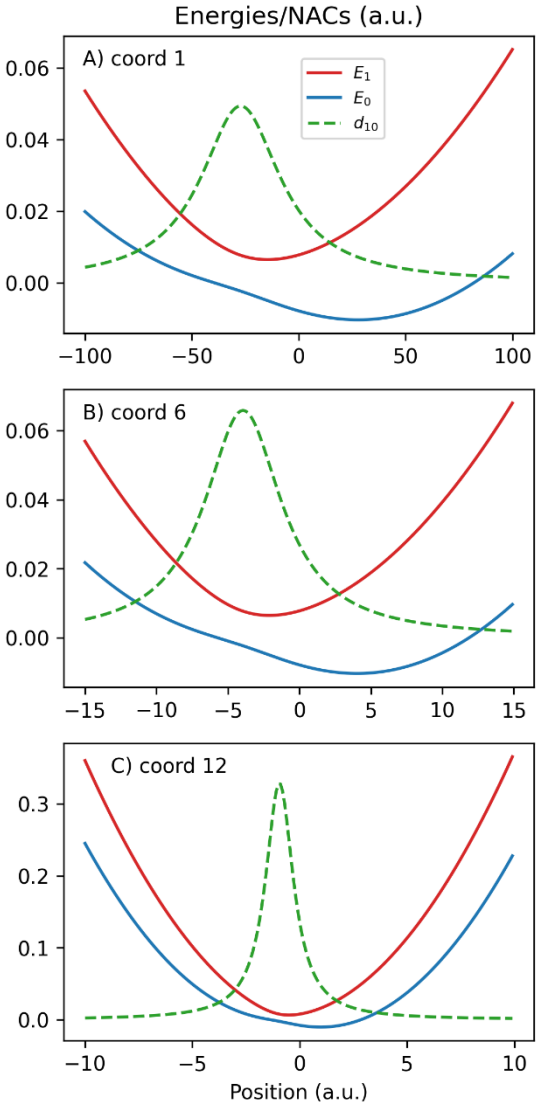

Figure 7 Cuts of the SBH model potential in adiabatic representation. Energies of E_0 and E_1 and the nonadiabatic coupling norm in a.u from state 1 to state 0. The presented d_{10} values are rescaled to fit with the energies. The panels show profiles along A) coordinate 1 ($\omega = 14cm^{-1}$), $d_{10}/20$; B) coordinate 6 ($\omega = 96cm^{-1}$), $d_{10}/15$; and C) coordinate 12 ($\omega = 400cm^{-1}$), $d_{10}/3$.

All the populations presented show the average value in the lines and the confidence interval of 95% in the shaded area. The averages and standard deviation were computed using the bootstrap method using 100000 resamples.

5 Application

5.1 Unidimensional systems

5.1.1 Tully 1: Simple avoided crossing

The simple avoided model is characterized by the potential energy surfaces coming reasonably close (≈ 0.27 eV) once but never crossing each other (Figure 6-A). Depending on the initial velocity, this can cause a partial transfer to the upper state.

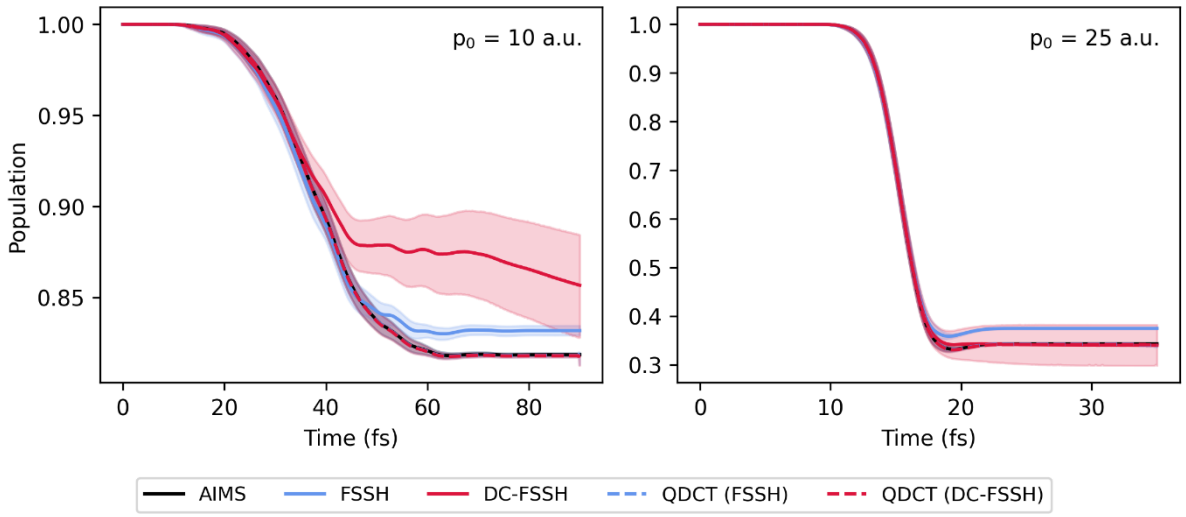

Figure 8 Lower state population for the simple avoided crossing Tully model. The initial condition was sampled around the momenta of 10 a.u. and 25 a.u. The shaded area in all curves represents a confidence interval of 95%.

In general, surface hopping should be performed with decoherence correction. We can see in Figure 8 that, in the low initial momentum, the DC-FSSH population underestimates the transfer, and even as the trajectories have already left the coupling region beyond 80 fs, the population is still not stabilized. Compared to the trajectories without decoherence correction, the confidence interval is much wider for the corrected trajectories. The original FSSH algorithm is much closer to the behavior of the AIMS population and the results found in previous work for this model.[47] When applied to both the trajectories generated by FSSH and DC-FSSH, QDCT recovers the AIMS population and, most importantly, does the same for both surface hopping outputs. The larger confidence interval in DC-FSSH is the effect of the decoherence correction tempering with the coefficients. In Supporting Information S4, there is a short discussion of this topic with an example.

In the case of higher initial momentum, where the particle behaves more like a classical particle and surface hopping should work better,[7,12] there is a good agreement between all methods. In this case, the DC-FSSH is closer to the reference than the original FSSH. Even with the improved result, the corrected decoherence still has a wider confidence interval than the other methods. Once again, QDCT can improve the population of the FSSH and not alter the result of DC-FSSH other than reducing the confidence interval.

The take-home message here (and in the following sections) is not that QDCT corrects DC-FSSH to return uncorrected FSSH, but that QDCT will return satisfactory results no matter the quality of the initial surface hopping basis we have.

5.1.2 Tully 2: Dual avoided crossing

The second of the Tully models is the dual avoided crossing, characterized by two sequential regions of high coupling where the potential energy surfaces approach each other (Figure 6-B). The small interval between the pair of couplings makes it possibly the hardest of the three models.[48,55]

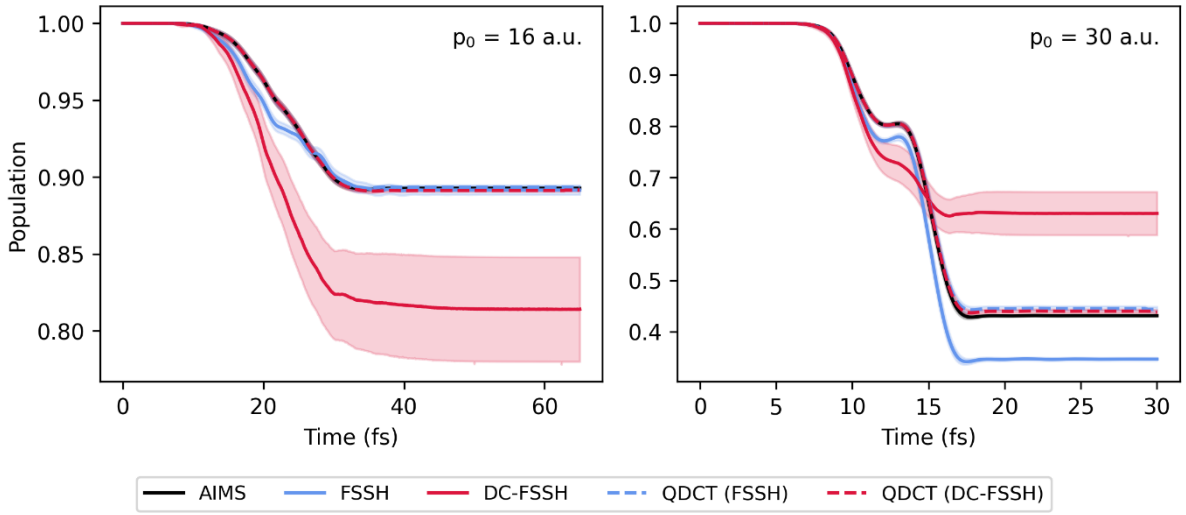

Figure 9 Lower state population for the dual avoided crossing Tully. The initial condition was sampled around the momenta of 16 a.u. and 30 a.u. The shaded area in all curves represents a confidence interval of 95%.

Once again, Figure 9 shows that using decoherence correction returns the asymptotic population 0.1 smaller than the reference for the lower momentum. On the other hand, despite having a slight difference in the transfer region, the original FSSH agrees with the AIMS asymptotic result.

In the high initial momentum simulations, the DC-FSSH disagrees even more with the reference. In this case, even the original FSSH disagrees with the AIMS result. The difficulty of FSSH in dealing with the sequential coupling regions has already been observed for this model.[48] When this system reaches the second coupling region, the fine control of the decoherence should influence the remaining

transfer between states. It could be related to the large discrepancy between this system's expected behavior and what is observed with DC-FSSH. Also, in this case, the QDCT recovers the AIMS result for both initial momenta and for both sets of surface hopping trajectories.

5.1.3 Tully 3: Extended coupling with reflection

The last unidimensional model starts in a region where the upper and lower electronic surfaces are degenerated. They pass through a coupling region, and the energies separate (Figure 6-C). If the trajectories that go through the upper state do not have enough kinetic energy, they are reflected and cause a second wave of population transfer, as can be seen in Figure 10.

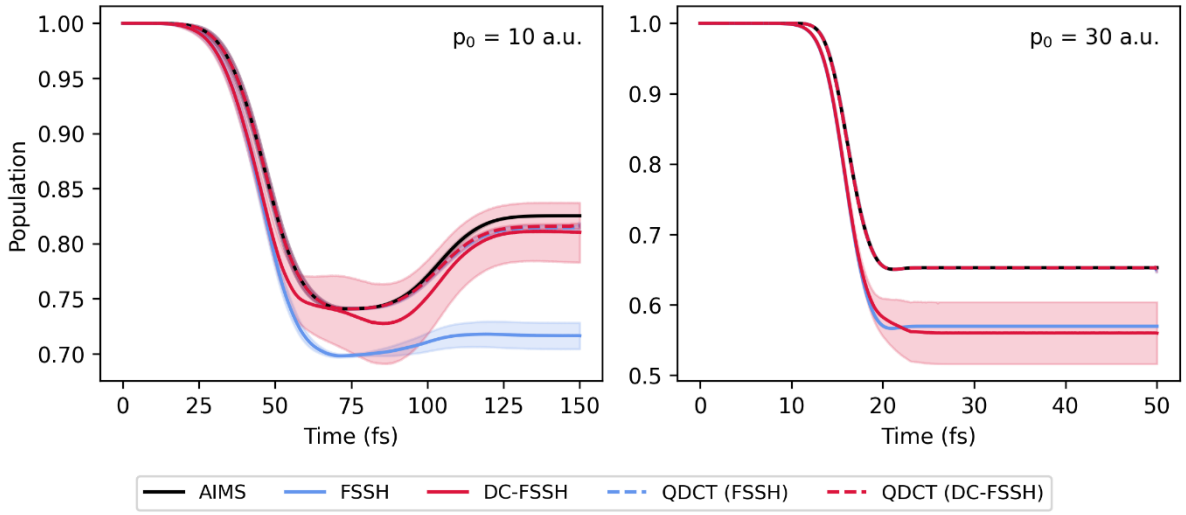

Figure 10 Lower state population for the simple avoided crossing Tully model. The initial condition was sampled around the momenta of 10 a.u. and 30 a.u. The shaded area in all curves represents a confidence interval of 95%.

For the low momentum case, most of the methods recover the population being transferred back to the lower state when the trajectories in the upper state are reflected. DC-FSSH has a slightly different profile from the reference but agrees with it overall. Original FSSH almost has no population being transferred back and has a wider confidence interval than observed in the other models. In the high-momentum case, the trajectories have enough kinetic energy to overcome the barrier in the upper state. Once the initial transfer is completed, the populations remain constant. Curiously, in this case, both surface hopping results agree among themselves but deviate from the reference. Once again, QDCT approximates the reference well, with a slight deviation in the low momentum case.

5.2 Multidimensional system

Although testing new methods in the Tully models is standard practice in the development of nonadiabatic dynamics, they are all unidimensional. To be practical, QDCT should also be able to deal with larger systems. This creates a problem that uncorrelated trajectories in higher dimensions will

rarely, if ever, have a significant overlap, which is essential for communication and population transfer between them. The Supporting Information S5 exemplifies how the overlap falls with increasing system dimensionality. The interpolated trajectories are required for the method to keep working in this scenario.

The Spin-Boson Hamiltonian is a family of models used to test nonadiabatic dynamic methods with the feature that its dimensionality can be arbitrarily increased. It linearly couples a two-state system (analogous to a spin-half system) to a bath of harmonic oscillator modes (the bosons). Due to its flexibility and rich dynamics, SBH has played a central role in the discussion of phenomena ranging from decoherence to nonadiabatic dynamics.[56] SBH is defined in terms of diabatic potentials for the bosonic modes. However, for surface hopping and multiple spawning, we move to the adiabatic representation (see Supporting Information S3). In this representation, the SBH model gives rise to two-state, multidimensional potential energy surfaces with significant anharmonicities and crossings analogous to a molecular system.

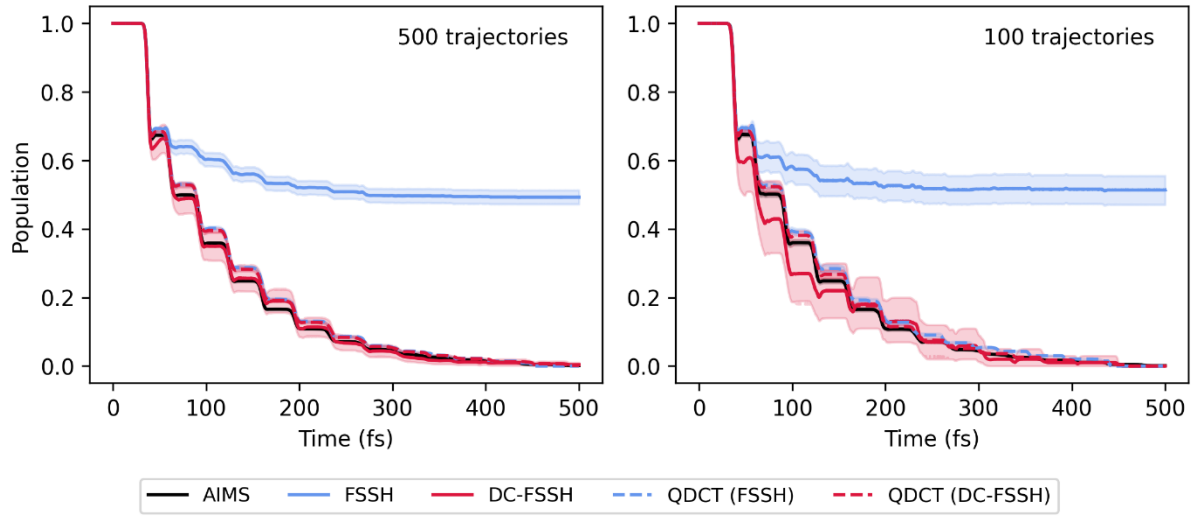

Figure 11 Upper state population for the SBH model using 500 trajectories (left) and 100 (right). The shaded area in all curves represents a confidence interval of 95%.

In the SBH model, we can see from Figure 11-left that the decoherence correction makes a difference and allows surface hopping to recover the correct result. This contrasts with the original FSSH, which considerably underestimates the population transfer, with an asymptotic population for the upper state above 50% at the end of the simulation. This illustrates a more realistic situation where decoherence corrections are essential. Although most methods agree well, DC-FSSH is generally closer to the reference population than the QDCT-corrected dynamics. In this case, the agreement of the different methods can be used to increase confidence in the result.

The result from Figure 11-left is from a converged simulation with 500 trajectories. Due to the cost of the single-point calculations, it is uncommon to see such many trajectories for an *ab initio* method. If,

instead, we take only the first 100 trajectories of AIMS and (DC-)FSSH to average and to give as input to QDCT, Figure 11-right shows how one can take advantage of the faster convergence of the multiple spawning method to improve the statistics of the surface hopping results. In this case, AIMS and QDCT give essentially the same result with the smaller number of trajectories as they did with the larger one. At the same time, DC-FSSH overestimates the population transfer in the first half of the simulation. The original FSSH shows a good convergence to a wrong result, showing that just ensuring convergence does not guarantee the quality of the result. The example of Figure 11-right is likely the closest to an actual application of the method, considering the number of trajectories used and that it is a multidimensional system. It does not show a significant improvement over DC-FSSH results but still converges well with the number of trajectories.

6 Conclusion

We have shown here the first steps of QDCT, a strategy to post-process surface hopping dynamics to obtain results at multiple spawning levels. QDCT helps to detect and correct potential problems in surface hopping. It can, for instance, be used as a method to recover decoherence effects in an over-coherent simulation. Even when QDCT leads to the same result as surface hopping, it comes at almost no extra cost since QDCT requires no new electronic structure calculation and increases confidence in the original simulation. If, on the other hand, the methods disagree in the behavior of the dynamics, QDCT can point to a problematic system that should be studied further, revealing possible problems with an analysis that would be otherwise considered correct.

The collection of unidimensional cases shows how, in some cases, the surface hopping dynamics can converge to an incorrect result. For a new system, there is no way to determine that other than by comparing it with different dynamics methods. In a multidimensional scenario, especially with heavier atoms, the system is supposed to approach classical behavior more, which is reflected in the vast success of surface hopping methods. Yet, approximations or corrections are necessary. Some should fare better in one type of system and worse in others. QDCT approaches this problem from a different perspective and is not susceptible to those approximations. Given the non-stochastic nature of the method and the increase of the basis size during the propagation, QDCT inherits from multiple spawning its improved convergence with the number of initial conditions, which can also be leveraged to improve the confidence in the initial results from surface hopping.

This post-process method inherit the problems of energy conservation of frozen Gaussian propagation used in AIMS,[57,58] but we also have the fact that the classical trajectories will have, in general, different total energies, as chosen in the initial condition generation of the surface hopping trajectories. In that case, the total energy of each simulation will be within the range of total energies of the trajectories, with a particular case that the expected value of the energy will be a weighted average of the energies of each trajectory when the overlap between all trajectories is negligible.

The quality of FSSH results depends significantly on how the electronic coefficients are propagated and corrected along the simulation. They will then only affect the classical trajectories by influencing the hopping points. QDCT is indifferent to those coefficients from surface hopping. As long as there are enough trajectories and the electronic structure used is reliable, the method should be able to approximate AIMS, as has been shown.

Although our entire discussion has focused on post-processing FSSH trajectories, QDCT can work on any surface hopping basis, stochastic[59] or deterministic,[60] even when nonadiabatic coupling vectors are not available, such as in curvature-based approaches[61–63] or global probability estimates.[64–68] In this case, however, it becomes necessary to modify the coefficient equation of motion (Eq. (5)) to replace the nonadiabatic coupling with the time derivative coupling.[34,69]

QDCT depends on a series of approximations. While some are more established, such as the BAT approximation, some can still be crude and invite extensive testing and refinement, particularly the interpolated trajectories. We plan to have our multiple spawning reference script interfaced with electronic structure codes to allow testing with real molecules. We will also investigate how the train of trajectories[37,40] and linear dependence removal[70] can improve the robustness of the QDCT method.

Although we have exclusively used QDCT to deliver results at a multiple-spawning calculation level, it is not restricted to trajectory spawning. It should be possible to emulate any strategy that uses Gaussian functions as a basis to propagate the TDSE: trains of trajectories and widths propagation, for example. Thus, in principle, we could devise QDCT versions that would aim to assess and improve the surface hopping quality against other quantum dynamics levels.

Acknowledgments

The authors thank the funding provided by the European Research Council (ERC) Advanced grant SubNano (Grant agreement 832237). The Centre de Calcul Intensif d'Aix-Marseille is acknowledged for granting access to its high-performance computing resources.

Author contributions

R.S.M.: conceptualization (equal), formal analysis (lead), investigation (lead), methodology (equal), software (lead), visualization (lead), writing – original draft (lead), and writing – review & editing (equal). S.M.: conceptualization (equal), methodology (equal), supervision (equal), and writing – review & editing (equal). M.B.: conceptualization (equal), funding acquisition (lead), methodology (equal), project administration (lead), supervision (equal), and writing – review & editing (equal).

Data availability

The code is available as open source but still in development at https://gitlab.com/rafaelcpii93/qdct.

Associated Content

Supporting Information available. It contains the derivation of the AIMS equations of motion, the analytical models, and a complementary discussion to the paper.

References

(1) Heller, E. J. Time Dependent Variational Approach to Semiclassical Dynamics. *J. Chem. Phys.* **1976**, *64* (1), 63–73. https://doi.org/10.1063/1.431911.
(2) Meyer, H. D.; Miller, W. H. A Classical Analog for Electronic Degrees of Freedom in Nonadiabatic Collision Processes. *J. Chem. Phys.* **1979**, *70* (7), 3214–3223. https://doi.org/10.1063/1.437910.
(3) Agostini, F.; Curchod, B. F. E. Different Flavors of Nonadiabatic Molecular Dynamics. *WIREs Comput. Mol. Sci.* **2019**, *9* (5), e1417. https://doi.org/10.1002/wcms.1417.
(4) Martinez, T. J.; Ben-Nun, M.; Levine, R. D. Multi-Electronic-State Molecular Dynamics: A Wave Function Approach with Applications. *J. Phys. Chem.* **1996**, *100* (19), 7884–7895. https://doi.org/10.1021/jp953105a.
(5) Meyer, H.-D.; Manthe, U.; Cederbaum, L. S. The Multi-Configurational Time-Dependent Hartree Approach. *Chem. Phys. Lett.* **1990**, *165* (1), 73–78. https://doi.org/10.1016/0009-2614(90)87014-I.
(6) Shalashilin, D. V. Quantum Mechanics with the Basis Set Guided by Ehrenfest Trajectories: Theory and Application to Spin-Boson Model. *J. Chem. Phys.* **2009**, *130* (24), 244101. https://doi.org/10.1063/1.3153302.
(7) Tully, J. C. Molecular Dynamics with Electronic Transitions. *J. Chem. Phys.* **1990**, *93* (2), 1061–1071. https://doi.org/10.1063/1.459170.
(8) Worth, G. A.; Robb, M. A.; Burghardt, I. A Novel Algorithm for Non-Adiabatic Direct Dynamics Using Variational Gaussian Wavepackets. *Faraday Discuss.* **2004**, *127*, 307–323. https://doi.org/10.1039/b314253a.
(9) Crespo-Otero, R.; Barbatti, M. Recent Advances and Perspectives on Nonadiabatic Mixed Quantum-Classical Dynamics. *Chemical Reviews*, 2018, *118*, 7026–7068. https://doi.org/10.1021/acs.chemrev.7b00577.
(10) Barbatti, M. Nonadiabatic Dynamics with Trajectory Surface Hopping Method. *Wiley Interdiscip. Rev. Comput. Mol. Sci.* **2011**, *1* (4), 620–633. https://doi.org/10.1002/wcms.64.
(11) Mukherjee, S.; Mattos, R. S.; Toldo, J. M.; Lischka, H.; Barbatti, M. Prediction Challenge: Simulating Rydberg Photoexcited Cyclobutanone with Surface Hopping Dynamics Based on Different Electronic Structure Methods. *J. Chem. Phys.* **2024**, *160* (15), 154306. https://doi.org/10.1063/5.0203636.
(12) Subotnik, J. E.; Ouyang, W.; Landry, B. R. Can We Derive Tully's Surface-Hopping Algorithm from the Semiclassical Quantum Liouville Equation? Almost, but Only with Decoherence. *J. Chem. Phys.* **2013**, *139* (21), 214107. https://doi.org/10.1063/1.4829856.
(13) Dupuy, L.; Rikus, A.; Maitra, N. T. Exact-Factorization-Based Surface Hopping without Velocity Adjustment. *J. Phys. Chem. Lett.* **2024**, *15* (10), 2643–2649. https://doi.org/10.1021/acs.jpclett.4c00115.
(14) Sindhu, A.; Jain, A. Benchmarking the Surface Hopping Method to Include Nuclear Quantum Effects. *J. Chem. Theory Comput.* **2021**, *17* (2), 655–665. https://doi.org/10.1021/acs.jctc.0c01065.
(15) Martinez, T. J.; Ben-Nun, M.; Ashkenazi, G. Classical/Quantal Method for Multistate Dynamics: A Computational Study. *J. Chem. Phys.* **1996**, *104* (8), 2847–2856. https://doi.org/10.1063/1.471108.

(16) Martínez, T. J.; Levine, R. D. Non-Adiabatic Molecular Dynamics: Split-Operator Multiple Spawning with Applications to Photodissociation. *J. Chem. Soc. Faraday Trans.* **1997**, *93* (5), 941–947. https://doi.org/10.1039/A605958I.
(17) Heller, E. J. Frozen Gaussians: A Very Simple Semiclassical Approximation. *J. Chem. Phys.* **1981**, *75* (6), 2923–2931. https://doi.org/10.1063/1.442382.
(18) Worth, G. A.; Robb, M. A.; Lasorne, B. Solving the Time-Dependent Schrödinger Equation for Nuclear Motion in One Step: Direct Dynamics of Non-Adiabatic Systems. *Mol. Phys.* **2008**, *106* (16–18), 2077–2091. https://doi.org/10.1080/00268970802172503.
(19) Leggett, A. J.; Chakravarty, S.; Dorsey, A. T.; Fisher, M. P. A.; Garg, A.; Zwerger, W. Dynamics of the Dissipative Two-State System. *Rev. Mod. Phys.* **1987**, *59* (1), 1–85. https://doi.org/10.1103/RevModPhys.59.1.
(20) Fabiano, E.; Keal, T. W.; Thiel, W. Implementation of Surface Hopping Molecular Dynamics Using Semiempirical Methods. *Chem. Phys.* **2008**, *349* (1), 334–347. https://doi.org/10.1016/j.chemphys.2008.01.044.
(21) Shu, Y.; Truhlar, D. G. Decoherence and Its Role in Electronically Nonadiabatic Dynamics. *J. Chem. Theory Comput.* **2023**. https://doi.org/10.1021/acs.jctc.2c00988.
(22) Bittner, E. R.; Rossky, P. J. Quantum Decoherence in Mixed Quantum-classical Systems: Nonadiabatic Processes. *J. Chem. Phys.* **1995**, *103* (18), 8130–8143. https://doi.org/10.1063/1.470177.
(23) Granucci, G.; Persico, M.; Zoccante, A. Including Quantum Decoherence in Surface Hopping. *J. Chem. Phys.* **2010**, *133* (13), 134111. https://doi.org/10.1063/1.3489004.
(24) Subotnik, J. E.; Shenvi, N. A New Approach to Decoherence and Momentum Rescaling in the Surface Hopping Algorithm. *J. Chem. Phys.* **2011**, *134* (2). https://doi.org/10.1063/1.3506779.
(25) Zhu, C.; Nangia, S.; Jasper, A. W.; Truhlar, D. G. Coherent Switching with Decay of Mixing: An Improved Treatment of Electronic Coherence for Non-Born–Oppenheimer Trajectories. *J. Chem. Phys.* **2004**, *121* (16), 7658–7670. https://doi.org/10.1063/1.1793991.
(26) Ben-Nun, M.; Quenneville, J.; Martínez, T. J. Ab Initio Multiple Spawning: Photochemistry from First Principles Quantum Molecular Dynamics. *J. Phys. Chem. A* **2000**, *104* (22), 5172–5175. https://doi.org/10.1021/jp994174i.
(27) Mignolet, B.; Curchod, B. F. E. A Walk through the Approximations of Ab Initio Multiple Spawning. *J. Chem. Phys.* **2018**, *148* (13). https://doi.org/10.1063/1.5022877.
(28) Curchod, B. F. E.; Glover, W. J.; Martínez, T. J. SSAIMS—Stochastic-Selection Ab Initio Multiple Spawning for Efficient Nonadiabatic Molecular Dynamics. *J. Phys. Chem. A* **2020**, *124* (30), 6133–6143. https://doi.org/10.1021/acs.jpca.0c04113.
(29) Lassmann, Y.; Curchod, B. F. E. AIMSWISS-Ab Initio Multiple Spawning with Informed Stochastic Selections. *J. Chem. Phys.* **2021**, *154* (21), 211106. https://doi.org/10.1063/5.0052118.
(30) Virshup, A. M.; Levine, B. G.; Martínez, T. J. Steric and Electrostatic Effects on Photoisomerization Dynamics Using QM/MM Ab Initio Multiple Spawning. *Theor. Chem. Acc.* **2014**, *133* (7), 1506. https://doi.org/10.1007/s00214-014-1506-5.
(31) Thompson, A. L.; Punwong, C.; Martínez, T. J. Optimization of Width Parameters for Quantum Dynamics with Frozen Gaussian Basis Sets. *Chem. Phys.* **2010**, *370* (1–3), 70–77. https://doi.org/10.1016/j.chemphys.2010.03.020.
(32) Born, M.; Huang, K. *Dynamical Theory of Crystal Lattices*, Repr.; The international series of monographs on physics; Clarendon Pr: Oxford, 1954.
(33) Ben-Nun, M.; Martínez, T. J. Nonadiabatic Molecular Dynamics: Validation of the Multiple Spawning Method for a Multidimensional Problem. *J. Chem. Phys.* **1998**, *108* (17), 7244–7257. https://doi.org/10.1063/1.476142.

(34) Fedorov, D. A.; Seritan, S.; Fales, B. S.; Martínez, T. J.; Levine, B. G. PySpawn: Software for Nonadiabatic Quantum Molecular Dynamics. *J. Chem. Theory Comput.* **2020**, *16* (9), 5485–5498. https://doi.org/10.1021/acs.jctc.0c00575.
(35) Ben-Nun, M.; Martínez, T. J. Exploiting Temporal Nonlocality to Remove Scaling Bottlenecks in Nonadiabatic Quantum Dynamics. *J. Chem. Phys.* **1999**, *110* (9), 4134–4140. https://doi.org/10.1063/1.478297.
(36) Curchod, B. F. E.; Martínez, T. J. Ab Initio Nonadiabatic Quantum Molecular Dynamics. *Chem. Rev.* **2018**, *118* (7), 3305–3336. https://doi.org/10.1021/acs.chemrev.7b00423.
(37) Makhov, D. V.; Glover, W. J.; Martinez, T. J.; Shalashilin, D. V. Ab Initio Multiple Cloning Algorithm for Quantum Nonadiabatic Molecular Dynamics. *J. Chem. Phys.* **2014**, *141* (5). https://doi.org/10.1063/1.4891530.
(38) Saller, M. A. C.; Habershon, S. Quantum Dynamics with Short-Time Trajectories and Minimal Adaptive Basis Sets. *J. Chem. Theory Comput.* **2017**, *13* (7), 3085–3096. https://doi.org/10.1021/acs.jctc.7b00021.
(39) Barbatti, M. Velocity Adjustment in Surface Hopping: Ethylene as a Case Study of the Maximum Error Caused by Direction Choice. *J. Chem. Theory Comput.* **2021**, *17* (5), 3010–3018. https://doi.org/10.1021/acs.jctc.1c00012.
(40) Shalashilin, D. V.; Child, M. S. Basis Set Sampling in the Method of Coupled Coherent States: Coherent State Swarms, Trains, and Pancakes. *J. Chem. Phys.* **2008**, *128* (5), 1–7. https://doi.org/10.1063/1.2828509.
(41) Kwon, H.-Y.; Morrow, Z.; Kelley, C. T.; Jakubikova, E. Interpolation Methods for Molecular Potential Energy Surface Construction. *J. Phys. Chem. A* **2021**, *125* (45), 9725–9735. https://doi.org/10.1021/acs.jpca.1c06812.
(42) Dral, P. O.; Ge, F.; Hou, Y.-F.; Zheng, P.; Chen, Y.; Barbatti, M.; Isayev, O.; Wang, C.; Xue, B.-X.; Pinheiro Jr, M.; Su, Y.; Dai, Y.; Chen, Y.; Zhang, L.; Zhang, S.; Ullah, A.; Zhang, Q.; Ou, Y. MLatom 3: A Platform for Machine Learning-Enhanced Computational Chemistry Simulations and Workflows. *J. Chem. Theory Comput.* **2024**, *20* (3), 1193–1213. https://doi.org/10.1021/acs.jctc.3c01203.
(43) Toniolo, A.; Ciminelli, C.; Persico, M.; Martínez, T. J. Simulation of the Photodynamics of Azobenzene on Its First Excited State: Comparison of Full Multiple Spawning and Surface Hopping Treatments. *J. Chem. Phys.* **2005**, *123* (23), 234308. https://doi.org/10.1063/1.2134705.
(44) Barbatti, M.; Bondanza, M.; Crespo-Otero, R.; Demoulin, B.; Dral, P. O.; Granucci, G.; Kossoski, F.; Lischka, H.; Mennucci, B.; Mukherjee, S.; Pederzoli, M.; Persico, M.; Pinheiro Jr, M.; Pittner, J.; Plasser, F.; Sangiogo Gil, E.; Stojanovic, L. Newton-X Platform: New Software Developments for Surface Hopping and Nuclear Ensembles. *J. Chem. Theory Comput.* **2022**, *18* (11), 6851–6865. https://doi.org/10.1021/acs.jctc.2c00804.
(45) Granucci, G.; Persico, M. Critical Appraisal of the Fewest Switches Algorithm for Surface Hopping. *J. Chem. Phys.* **2007**, *126* (13), 134114. https://doi.org/10.1063/1.2715585.
(46) Lee, H.-W. Wigner Trajectories of a Gaussian Wave Packet Perturbed by a Weak Potential. *Found. Phys.* **1992**, *22* (8), 995–1010. https://doi.org/10.1007/BF00733392.
(47) Agostini, F.; Min, S. K.; Abedi, A.; Gross, E. K. U. Quantum-Classical Nonadiabatic Dynamics: Coupled- vs Independent-Trajectory Methods. *J. Chem. Theory Comput.* **2016**, *12* (5), 2127–2143. https://doi.org/10.1021/acs.jctc.5b01180.
(48) Miao, G.; Subotnik, J. Revisiting the Recoherence Problem in the Fewest Switches Surface Hopping Algorithm. *J. Phys. Chem. A* **2019**, *123* (26), 5428–5435. https://doi.org/10.1021/acs.jpca.9b03188.
(49) Ibele, L. M.; Lassmann, Y.; Martínez, T. J.; Curchod, B. F. E. Comparing (Stochastic-Selection) Ab Initio Multiple Spawning with Trajectory Surface Hopping for the

Photodynamics of Cyclopropanone, Fulvene, and Dithiane. *J. Chem. Phys.* **2021**, *154* (10). https://doi.org/10.1063/5.0045572.
(50) Ibele, L. M.; Curchod, B. F. E. A Molecular Perspective on Tully Models for Nonadiabatic Dynamics. *Phys. Chem. Chem. Phys.* **2020**, *22* (27), 15183–15196. https://doi.org/10.1039/D0CP01353F.
(51) Toldo, J. M.; Mattos, R. S.; Pinheiro, M.; Mukherjee, S.; Barbatti, M. Recommendations for Velocity Adjustment in Surface Hopping. *J. Chem. Theory Comput.* **2024**, *20* (2), 614–624. https://doi.org/10.1021/acs.jctc.3c01159.
(52) Garg, A.; Onuchic, J. N.; Ambegaokar, V. Effect of Friction on Electron Transfer in Biomolecules. *J. Chem. Phys.* **1985**, *83* (9), 4491–4503. https://doi.org/10.1063/1.449017.
(53) Mac Kernan, D.; Ciccotti, G.; Kapral, R. Surface-Hopping Dynamics of a Spin-Boson System. *J. Chem. Phys.* **2002**, *116* (6), 2346–2353. https://doi.org/10.1063/1.1433502.
(54) Weiss, U. *Quantum Dissipative Systems*, 2nd ed.; Series in Modern Condensed Matter Physics; WORLD SCIENTIFIC, 1999; Vol. 10. https://doi.org/10.1142/4239.
(55) Shenvi, N.; Subotnik, J. E.; Yang, W. Phase-Corrected Surface Hopping: Correcting the Phase Evolution of the Electronic Wavefunction. *J. Chem. Phys.* **2011**, *135* (2), 024101. https://doi.org/10.1063/1.3603447.
(56) Schlosshauer, M. *Decoherence and the Quantum-to-Classical Transition*; Springer, 2007.
(57) Ibele, L.; Memhood, A.; Levine, B. G.; Avagliano, D. Ab Initio Multiple Spawning Nonadiabatic Dynamics with Different CASPT2 Flavors: A Fully Open-Source PySpawn/OpenMolcas Interface. ChemRxiv July 2, 2024. https://doi.org/10.26434/chemrxiv-2024-s8z45.
(58) Habershon, S. Linear Dependence and Energy Conservation in Gaussian Wavepacket Basis Sets. *J. Chem. Phys.* **2012**, *136* (1), 014109. https://doi.org/10.1063/1.3671978.
(59) Wang, L.; Akimov, A.; Prezhdo, O. V. Recent Progress in Surface Hopping: 2011–2015. *J. Phys. Chem. Lett.* **2016**, *7* (11), 2100–2112. https://doi.org/10.1021/acs.jpclett.6b00710.
(60) Mannouch, J. R.; Richardson, J. O. A Mapping Approach to Surface Hopping. *J. Chem. Phys.* **2023**, *158* (10), 104111. https://doi.org/10.1063/5.0139734.
(61) T. do Casal, M.; Toldo, J. M.; Pinheiro Jr, M.; Barbatti, M. Fewest Switches Surface Hopping with Baeck-An Couplings. *Open Res. Eur.* **2021**, *1*, 49. https://doi.org/10.12688/openreseurope.13624.1.
(62) Shu, Y.; Zhang, L.; Chen, X.; Sun, S.; Huang, Y.; Truhlar, D. G. Nonadiabatic Dynamics Algorithms with Only Potential Energies and Gradients: Curvature-Driven Coherent Switching with Decay of Mixing and Curvature-Driven Trajectory Surface Hopping. *J. Chem. Theory Comput.* **2022**, *18* (3), 1320–1328. https://doi.org/10.1021/acs.jctc.1c01080.
(63) Shu, Y.; Truhlar, D. G. Generalized Semiclassical Ehrenfest Method: A Route to Wave Function-Free Photochemistry and Nonadiabatic Dynamics with Only Potential Energies and Gradients. *J. Chem. Theory Comput.* **2024**. https://doi.org/10.1021/acs.jctc.4c00424.
(64) Belyaev, A. K.; Lasser, C.; Trigila, G. Landau–Zener Type Surface Hopping Algorithms. *J. Chem. Phys.* **2014**, *140* (22), 224108. https://doi.org/10.1063/1.4882073.
(65) Suchan, J.; Janoš, J.; Slavíček, P. Pragmatic Approach to Photodynamics: Mixed Landau–Zener Surface Hopping with Intersystem Crossing. *J. Chem. Theory Comput.* **2020**, *16* (9), 5809–5820. https://doi.org/10.1021/acs.jctc.0c00512.
(66) Xie, W.; Sapunar, M.; Došlić, N.; Sala, M.; Domcke, W. Assessing the Performance of Trajectory Surface Hopping Methods: Ultrafast Internal Conversion in Pyrazine. *J. Chem. Phys.* **2019**, *150* (15), 154119. https://doi.org/10.1063/1.5084961.
(67) Yue, L.; Yu, L.; Xu, C.; Lei, Y.; Liu, Y.; Zhu, C. Benchmark Performance of Global Switching versus Local Switching for Trajectory Surface Hopping Molecular Dynamics Simulation: Cis↔Trans Azobenzene Photoisomerization. *ChemPhysChem* **2017**, *18* (10), 1274–1287. https://doi.org/10.1002/cphc.201700049.

(68) Zhang, L.; Pios, S. V.; Martyka, M.; Ge, F.; Hou, Y.-F.; Chen, Y.; Chen, L.; Jankowska, J.; Barbatti, M.; Dral, P. O. MLatom Software Ecosystem for Surface Hopping Dynamics in Python with Quantum Mechanical and Machine Learning Methods. *J. Chem. Theory Comput.* **2024**. https://doi.org/10.1021/acs.jctc.4c00468.
(69) Meek, G. A.; Levine, B. G. Evaluation of the Time-Derivative Coupling for Accurate Electronic State Transition Probabilities from Numerical Simulations. *J. Phys. Chem. Lett.* **2014**, *5* (13), 2351–2356. https://doi.org/10.1021/jz5009449.
(70) Joubert-Doriol, L. A Variational Approach for Linearly Dependent Moving Bases in Quantum Dynamics: Application to Gaussian Functions. *J. Chem. Theory Comput.* **2022**, *18* (10), 5799–5809. https://doi.org/10.1021/acs.jctc.2c00461.

For Table of Contents Only